Impact of Field Strength in Clinical Cardiac Magnetic Resonance Imaging

Impact of Field Strength in Clinical Cardiac Magnetic Resonance Imaging

Robert J. Holtackers, MSc,†‡ Joachim E. Wildberger, MD, PhD,*†*
Bernd J. Wintersperger, MD,§|| and Amedeo Chiribiri, MD, PhD‡¶

Abstract: Cardiac magnetic resonance imaging (MRI) is widely applied for the noninvasive assessment of cardiac structure and function, and for tissue characterization. For more than 2 decades, 1.5 T has been considered the field strength of choice for cardiac MRI. Although the number of 3-T systems significantly increased in the past 10 years and numerous new developments were made, challenges seem to remain that hamper a widespread clinical use of 3-T MR systems for cardiac applications. As the number of clinical cardiac applications is increasing, with each having their own benefits at both field strengths, no "holy grail" field strength exists for cardiac MRI that one should ideally use. This review describes the physical differences between 1.5 and 3 T, as well as the effect of these differences on major (routine) cardiac MRI applications, including functional imaging, edema imaging, late gadolinium enhancement, first-pass stress perfusion, myocardial mapping, and phase contrast flow imaging. For each application, the advantages and limitations at both 1.5 and 3 T are discussed. Solutions and alternatives are provided to overcome potential limitations. Finally, we briefly elaborate on the potential use of alternative field strengths (ie, below 1.5 T and above 3 T) for cardiac MRI and conclude with field strength recommendations for the future of cardiac MRI.

Key Words: cardiovascular disease, magnetic resonance imaging, cardiac magnetic resonance, field strength

(*Invest Radiol* 2021;56: 764–772)

Cardiac magnetic resonance imaging (MRI) is widely applied for the noninvasive assessment of cardiac morphology, global and regional cardiac function, and for detailed tissue characterization. Because of continued technical advancements and developments together with ever-growing research in recent decades, numerous new application scenarios have pushed the envelope for expanded clinical application of cardiac MRI. The advent of techniques, such as parallel imaging, compressed sensing, respiratory navigation, and motion correction, has enabled the application of real-time and free-breathing acquisitions with much improved patient comfort. Simultaneously, due to ongoing development and regulatory approval of MRI conditional cardiac devices and other implants, the patient population amenable to cardiac MRI is growing. A growing body of evidence based on large clinical trials supports the added benefit of cardiac MRI in various patient populations and, together with ongoing pharmacological developments, may impact patient management and therapy decisions. Nevertheless, despite the growing availability of capable scanners, the overall number of clinical cardiac MRI examinations remains limited compared with other modalities, such as echocardiography, computed tomography (CT), and single photon emission CT. Cost-efficiency and ease-of-use remain key determinants whether cardiac MRI, and its advanced capabilities will be further implemented into routine clinical care beyond academic centers.

Capital investment and service costs of MR systems largely scale with the strength of the system's external magnetic field. As such, selection of the appropriate field strength remains a crucial purchase decision. For the better part of the last quarter century, 1.5 T has been considered the "ideal" field strength for cardiac examinations. However, predominately based on the benefits of high-field MR in other noncardiac applications (eg, neuro, musculoskeletal), 3-T systems have become more widely operational in clinical routine settings.

The push toward higher field strength is generally based on a signal-to-noise ratio (SNR) benefit, as SNR increases proportionally with field strength.[1] Such gain generally proves beneficial for image acquisition acceleration with subsequent improvement in spatial and temporal resolution. Because of its exposure to various physiologic motion patterns, such improvement generally benefits cardiac MRI applications. However, the increase in SNR with higher field strength is accompanied by effects that may limit practical implementation of techniques. These include losses of homogeneity in both the main magnetic field (B_0) and radiofrequency (RF) field (B_1), increased energy deposit indicated by higher specific absorption rates (SARs), more pronounced and increased imaging artifacts, and increased attractive and rotational forces acting on ferromagnetic objects.

In this review, we not only discuss the basic differences of MR physics at 1.5 T versus 3 T and their effect on clinical cardiac MRI applications but also highlight solutions and/or alternatives to overcome potential limitations. The highlighted applications include morphologic imaging, functional imaging, perfusion imaging, as well as qualitative and quantitative tissue characterization. For each application, the specific advantages and limitations at 1.5 T and 3 T are discussed. Furthermore, we briefly elaborate on the potential use of alternative field strength (<1.5 T and >3 T) and potential other developments for cardiac MRI.

FUNCTIONAL IMAGING

Assessment of cardiac function and size using cine imaging is at center stage of almost every cardiac MRI examination.[2] Most commonly, retrospectively gated balanced steady-state free precession (bSSFP) sequences are used for cine imaging due to their high SNR and excellent flow-independent contrast-to-noise ratio (CNR) between blood and myocardium.[3] No significant differences in left ventricular (LV) functional parameters, such as ejection fraction, volumes, and mass were found between 1.5 T and 3 T when using bSSFP techniques.[4,5] The gain in SNR in cine imaging at 3 T[6] facilitates the use of higher acceleration factors when using parallel imaging. As a result of accelerated data sampling, the higher field strength allows for increased temporal (more cardiac phases acquired) or spatial (smaller

Received for publication April 1, 2021; and accepted for publication, after revision, June 1, 2021.

From the *Cardiovascular Research Institute Maastricht, Maastricht University; †Department of Radiology and Nuclear Medicine, Maastricht University Medical Centre, Maastricht, the Netherlands; ‡School of Biomedical Engineering and Imaging Sciences, King's College London, London, United Kingdom; §Department of Medical Imaging, Peter Munk Cardiac Centre, University Health Network; || Department of Medical Imaging, University of Toronto, Toronto, Ontario, Canada; and ¶Department of Cardiology, Guy's and St Thomas' NHS Foundation Trust, London, United Kingdom.

Conflicts of interest and sources of funding: none declared.

Correspondence to: Robert J. Holtackers, MSc, Department of Radiology and Nuclear Medicine, Maastricht University Medical Centre, PO Box 5800, 6202 AZ Maastricht, the Netherlands. E-mail: rob.holtackers@mumc.nl.

ISSN: 0020-9996/21/5611–0764
DOI: 10.1097/RLI.0000000000000809

voxel size) resolution, a reduction in breath-hold duration, or a combination of either. However, the theoretical SNR doubling at 3 T is partly offset by the longer T_1 and shortened T_2* relaxation times compared with 1.5 T.[7]

Besides the benefits, various challenges arise with bSSFP cine imaging at 3 T. The increased RF power required at 3 T, resulting in a 4-fold energy deposition compared with 1.5 T, generally limits the flip angle and also the minimal achievable repetition time (TR) due to SAR restrictions.[8] Furthermore, the shorter wavelength of the RF pulse causes increased B_1 inhomogeneity with more problematic penetration of deeper structures.[9] Apart from B_1 inhomogeneity, the B_0 inhomogeneity also increases at higher field strengths (by 2 ppm at 3 T).[8] Because of the resulting resonance frequency shifts, bSSFP techniques in particular are prone to repetitive "dark band" (off-resonance) artifacts that may substantially hamper image interpretation (Fig. 1). Although also appearing at 1.5 T, the distance between such bands is inversely proportional to the field strength and TR, and thus more commonly affecting the heart at 3 T. Besides high-order shimming capabilities on modern equipment, frequency scouting techniques determining the central frequency help reduce and shift respective artifacts outside the central field of view.[10] It is worth mentioning that these adjustments may not be sufficient for all slices in a multislice imaging stack. Furthermore, the applied frequency scouting sequence needs to match the TR of the subsequently used bSSFP cine sequence.

In the rare scenario of nondiagnostic bSSFP cine image quality due to dark band artifacts, standard spoiled gradient recalled echo (GRE) sequences can be applied.[2] However, as the contrast between blood and the myocardium in GRE cine is based on inflow of fresh magnetization (eg, blood), poor delineation results especially in cases of impaired cardiac function or regional wall motion abnormalities with slow blood flow.[11] The use of contrast agents may overcome this limitation and further enhance image contrast.[12] Because of the differences in wall segmentation, generally different normal range tables apply for GRE sequences.[11]

Beyond global function and volumetrics, assessment of myocardial mechanics with quantification of global and regional deformation has gained substantial attraction in recent years.[13] Besides dedicated cardiac MRI methods, such as tagging,[14] strain encoding (SENC),[15] and displacement encoding (DENSE),[16] feature tracking methods based on dedicated postprocessing analysis of routinely acquired bSSFP cine images allow for quantification of myocardial strain. Assessment of myocardial strain may provide important information in the assessment of dyssynchronous myocardial contraction and also enable identification of abnormalities before deterioration of global functional parameters such as ejection fraction. A limited body of evidence exists, showing that outcome prediction is similar when comparing feature tracking-based strain acquired at 1.5 T and 3 T, and that no significant differences were found in global values of longitudinal, radial, and circumferential strain.[17,18] Although such data are promising, optimization of image quality remains key to provide consistent feature tracking results. Overall, variation in feature tracking results seem to predominately originate from applied software packages,[19] number of slices used,[17] and observer experience.[20] Furthermore, various acceleration methods likely impact the "features" in cine imaging and may also affect feature tracking results.

EDEMA IMAGING

Edema imaging is commonly used for the discrimination between acute and chronic myocardial pathologies, as edema represents a fairly nonspecific and reversible response to myocardial injury.[21] Beside identification of affected myocardium in inflammatory pathologies, edema imaging not only allows differentiation of acute and chronic ischemic damage, but can also, in combination with late gadolinium enhancement (LGE) imaging, quantify the salvageable myocardium that has the potential to recover with timely revascularization.[22]

Qualitative edema imaging is typically based on a variety of widely available segmented T_2-weighted turbo spin echo (TSE) techniques combined with either short-tau inversion recovery (STIR), spectral presaturation inversion recovery (IR), or spectral attenuated IR for fat suppression. Suppression of signal from flowing blood with improvement of image quality is added by double inversion (nonselective/selective) black-blood preparation.[23] Alternatively, bright-blood T_2-weighted imaging sequences, such as a single-shot bSSFP sequence with added T_2 preparation (T_2-prepared bSSFP), can be used.[24] Another alternative includes a hybrid approach that combines conventional black-blood TSE and T_2-prepared bSSFP ($ACUT_2E$).[25] More recently, a novel single-shot bSSFP method was proposed with a preceding T_2 preparation module and STIR pulse (T_2STIR-bSSFP).[26] The longer T_2 relaxation times of the water-bound protons cause areas of edema to yield higher signal intensity on the T_2-weighted images and thereby appear

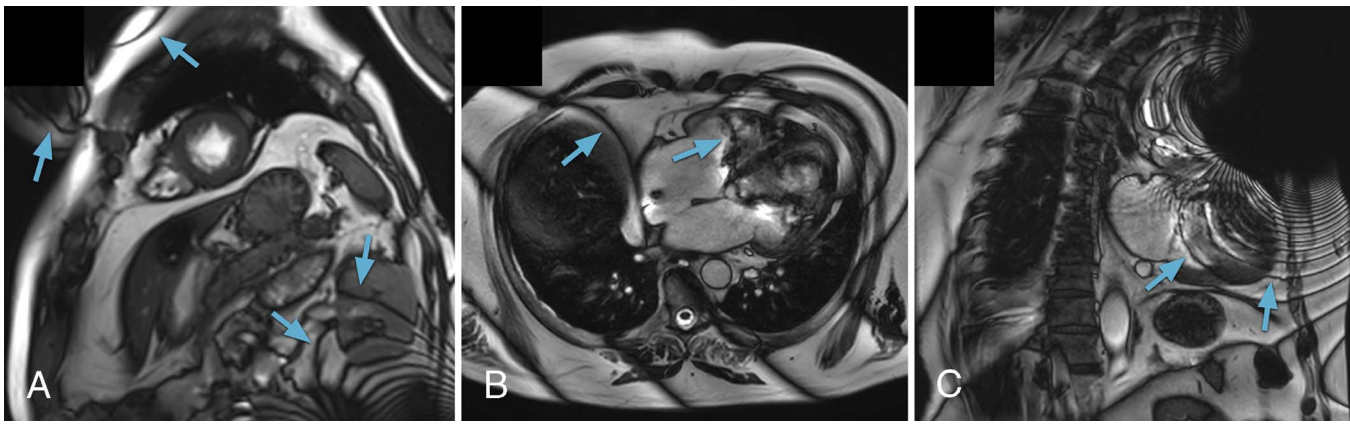

FIGURE 1. Balanced steady-state free precession (bSSFP) cine images acquired in multiple cardiac views. A, A short-axis view acquired at 3 T showing dark banding artifacts (indicated by arrows) near the edges of the image where the main magnetic field (B_0) is more heterogenous than in the isocenter, where the heart is located. B, A 4-chamber view acquired at 1.5 T showing extensive dark banding artifacts over the entire image due to the considerable B_0 field inhomogeneities caused by the presence of an implantable cardioverter-defibrillator (ICD). The orientation of the dark banding artifacts is strongly affected in the proximity of the generator, near the apex of the heart. The flowing blood inside the left and right ventricle causes the dark bands to move with the flow direction. C, A 2-chamber view acquired at 1.5 T showing a clear signal void above the heart due to the presence of an ICD. The metallic body of the ICD heavily disturbs the B_0 homogeneity, leading to circular dark banding artifacts over the left ventricle.

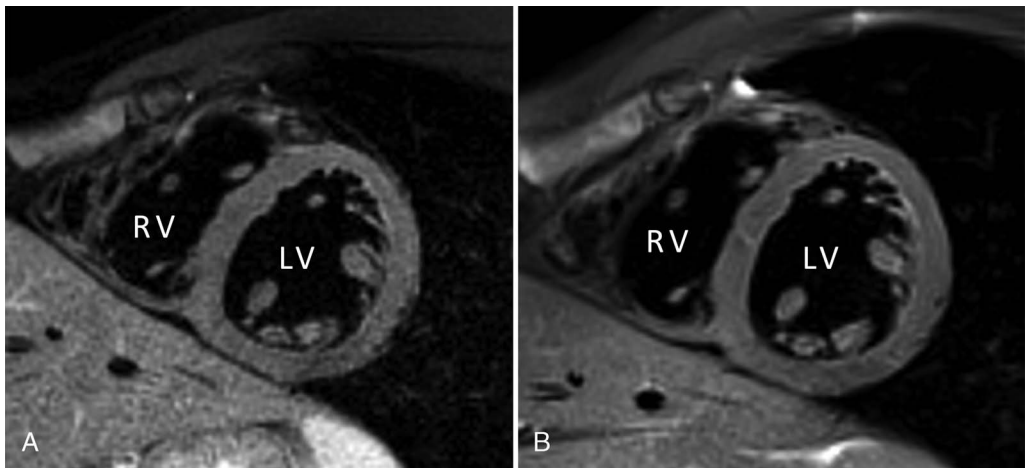

FIGURE 2. T_2-weighted black-blood turbo spin echo images acquired in a short-axis view at (A) 1.5 T and (B) 3 T (with identical spatial resolution). The increased field strength of 3 T comes with a significant gain in the signal-to-noise ratio, leading to a reduced noise level in the image. Image B, acquired at 3 T, shows significant less noise in the myocardial wall compared with image A, acquired at 1.5 T. LV, left ventricle; RV, right ventricle.

with increased signal intensity compared with normal myocardium and the blood pool.

Although T_2-weighted edema imaging can generally be performed on either field strength, various differences come into play. With the increased field strength at 3 T, edema imaging generally benefits from the overall SNR gain (Fig. 2). However, as the T_1 relaxation times of both myocardium and edema increase, the preparation pulses (eg, black-blood, fat suppression) are adjusted accordingly.[26] The prolongation of T_1 relaxation and the differences between normal and edematous myocardium increases, leading to further improved contrast at 3 T. Nevertheless, TSE techniques may generally encounter SAR limitations due to the repetitive refocusing pulses and T_2 preparation modules needed. In addition, the aforementioned increase in RF field inhomogeneity at 3 T may cause imperfect refocusing of the magnetization, with resulting signal variation across the myocardium (Fig. 3). Similarly, the increased B_0 inhomogeneity may result in inhomogeneous fat suppression across the area of interest or even result in suppression of myocardial signal in chemical shift–based fat saturation methods. Although STIR fat suppression is less susceptible to such field strength variation, the technique inherently results in lower SNR and may expose unwanted T_1-weighting.

As demonstrated previously, whenever applying methods that use bSSFP readouts, appropriate sequence adjustments with short TR, sufficient high-order shimming, or frequency adjustments are required to avoid or minimize effects from dark band artifacts at 3 T. At either field strength, the general limitations of qualitative T_2-weighted imaging apply. Although fairly sensitive for identification of focal myocardial edema, assessment of diffuse edematous changes remains challenging. Normalization can be performed using remote myocardium or skeletal muscle as reference; however, this may be hampered by systemic inflammatory processes or the need to use the standard body coil for homogenous signal distribution, which will result in a general SNR drop. Recently evolved quantitative methods may provide more objective measures of myocardial T_2 relaxation time changes (see further below).

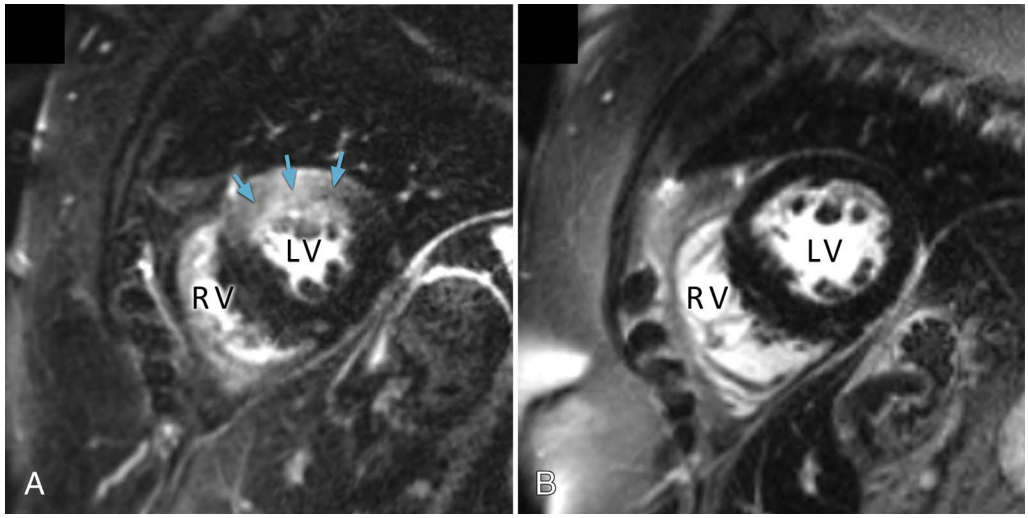

FIGURE 3. Late gadolinium enhancement images acquired in a short-axis view (A) before and (B) after high-order shimming of the radiofrequency (B_1) field at 3 T. Without adequate shimming, in particular at higher field strengths, the B_1 field is spatially varying. As a result, the flip angles experienced by the tissue also vary spatially, causing areas to appear brighter or darker based on their location. The arrows indicate the anterior section of the myocardial wall that appears enhanced compared with the rest of the myocardium (A). After adequate shimming, the same myocardial section is appearing normal again (B).

LATE GADOLINIUM ENHANCEMENT

Late gadolinium enhancement imaging has emerged as the noninvasive reference standard for the visualization of the myocardial interstitial space. Its ability to distinguish nonischemic replacement fibrosis and myocardial infarction scar from healthy viable myocardium is well established. Thus, LGE imaging is a highly important component of almost every cardiac MRI in patients with acquired cardiac diseases. The basic principle of LGE is the accumulation of extracellular gadolinium-based contract agents (GBCAs) contrast agent in areas of increased distribution volume. Underlying pathophysiologic processes include either cell membrane rupture (acute injury) or expansion of the interstitial space due to interstitial fibrosis, deposits, or edema. As a result of this GBCA "accumulation," using a strong T_1-weighted sequence ~10 to 20 minutes post-GBCA injection, areas with increased contrast concentration will appear hyperintense compared with normal myocardium. To further improve the contrast between normal and abnormal myocardium, segmented 2-dimensional (2D) IR techniques with either a spoiled GRE[27] or bSSFP[28] readout are in use during breath-held acquisitions. Alternatively, single-shot techniques with bSSFP readout may be used for patients with limited breath-holding capabilities and/or in the setting of arrhythmia.[29] More recent developments also use free-breathing 2D motion-corrected techniques,[30,31] free-breathing 3-dimensional (3D) techniques that allow for high isotropic spatial resolution,[32,33] and motion-corrected water-fat separated 3D techniques.[34]

There is a multitude of data demonstrating that LGE imaging can be performed on both 1.5 T and 3 T, and multiple studies also directly compared both field strengths. Regardless of whether a segmented GRE or single-shot bSSFP approach has been used for IR-prepared LGE imaging, 3 T demonstrated a significant increase in CNR between normal and infarcted myocardium for both chronic[29,35,36] and acute[37] myocardial infarction. Again, bSSFP readout techniques demonstrated more image artifacts at 3 T.[29] Regarding the extent of myocardial scar, infarct volume correlated well between 1.5 T and 3 T; however, individual patients demonstrated significant variation.[29,36]

With the increase of field strength, T_1 relaxation times of both myocardium and blood prolong. Furthermore, the "efficiency" to shorten T_1, expressed as R_1 relativity, of all clinically approved extracellular GBCAs in plasma is reduced by ~3% to 10% at 3 T compared with 1.5 T.[38] Overall, although no significant difference in T_1 relaxation times of myocardium or blood at 3 T versus 1.5 T appears directly after GBCA injection, after early contrast clearance and reaching a dynamic steady state intrinsic differences become apparent again with longer T_1 times for normal myocardium at 3 T compared with 1.5 T.[39] Thus, the inversion time required to null normal myocardium is typically ~50 milliseconds longer at 3 T than on 1.5 T.[35,37] The combination of these various effects at 3 T results in a significantly increased SNR and CNR of infarct scar as confirmed by several studies.[35–37,40]

Despite the previously listed benefits of LGE at 3 T, users also need to be aware of various potential misleading effects. Because of the general increased RF pulse inhomogeneity at 3 T, spatially varying inversion pulse flip angle may occur throughout the heart. As a result, the suppression of the myocardium may vary spatially and may mimic regions of diffuse LGE (similar as for "edema imaging" as shown in Fig. 3). Adiabatic inversion RF pulses may be applied to mitigate this limitation, resulting in more homogeneous magnetization inversion and as such more homogenous myocardial nulling.[41] Although RF power deposition is significantly increased at higher field strength, due to the sequence design, SAR limitations rarely occur in LGE imaging.

Regardless of the contrast between normal and infarcted myocardium, conventional LGE methods often experience poor scar-to-blood contrast. Various methods have been developed to increase scar-to-blood contrast.[42–45] Although not all have been evaluated at both fields strengths,[46] current results show that such methods were able to resolve cases with ambiguous conventional LGE, clearly distinguishing between patients with and without hyperintense areas at both 1.5 T and 3 T.[43,44]

FIRST-PASS STRESS PERFUSION IMAGING

Vasodilatory first-pass stress perfusion imaging has demonstrated high diagnostic accuracy and is clinically used for the detection of myocardial ischemia, alongside single photon emission CT, positron emission tomography, and echocardiography. Most commonly, first-pass perfusion imaging is performed during a peripheral GBCA bolus injection at peak vasodilatory stress (eg, adenosine, regadenoson, dipyridamole), as well as at rest. Areas of myocardium with reduced perfusion (most commonly due to hemodynamically significant epicardial coronary artery stenosis) demonstrate delayed signal intensity increase during the GBCA first pass and therefore appear hypointense. In clinical routine, myocardial coverage is typically ensured by at least 3 short axis slices for assessment of perfusion according to the standard 16 AHA LV segments.

Applied sequence techniques are generally based on electrocardiogram-triggered T_1-weighted saturation recovery techniques applying a 90-degree saturation pulse for precontrast signal nulling and adequate T_1 weighting for contrast bolus evaluation.[47] With the aim of appropriate evaluation/visualization of the first pass of the administered GBCA through cardiac chambers and LV myocardium, acquisition of each slice at every heart (eg, single heartbeat temporal resolution) beat is of outmost importance. Given this need for fast and rapid image acquisition, SNR and CNR become the main limiting factors in first-pass perfusion imaging.

Although, at 1.5 T, most commonly bSSFP, spoiled GRE, and also echo planar imaging readouts are used in perfusion imaging, at 3 T, the predominant choice is a spoiled GRE readout. In part, the latter reflects the general potential problems with bSSFP at 3 T that include high levels of energy deposition as well as the susceptibility to off-resonance artifacts (see previously).

It has been demonstrated that the use of the higher field strength is highly advantageous with respect to SNR gain and dynamic contrast enhancement ratios, as well as the signal intensity upslope of respective perfusion curves.[48] With the use of acceleration techniques, such gains can alternatively be reinvested into increased spatial resolution, higher temporal footprints, or improved myocardial coverage by acquisition of more slices. Thereby, cardiac perfusion MRI at 3 T is advantageous in comparison with 1.5 T for detecting myocardial ischemia with improved image quality and fewer extended dark-rim artifacts.[49] However, it is important to ensure that appropriate signal preparation is at use with composite saturation prepulses that are required to ensure an acceptable level of signal saturation and reduce inflow effects. Other problems negatively affecting the quality of perfusion images acquired at 3 T include the general aspects of imaging at higher field strengths, including reduction in main magnetic field homogeneity, the increase in RF power deposition, and the increase in susceptibility-based artifacts.[8]

Various clinical studies have highlighted that the previously described benefits of first-pass perfusion imaging at 3 T also demonstrate diagnostic impact. Cheng et al[50] have shown that stress perfusion cardiac MRI at 3 T is superior to imaging at 1.5 T for prediction of significant single-vessel and multivessel coronary disease. More recently, it has been reported that 3 T stress perfusion cardiac MRI showed higher diagnostic performance in patients with multivessel CAD compared with 1.5 T with coronary angiography as standard of reference.[51]

With most recent developments of automated quantitative analysis,[52] predominately made possible by application of artificial intelligence preprocessing and postprocessing,[53] further steps have been taken for more routine clinical application independent of user expertise. Although limited data comparing field strength are available, quantitative analysis has been shown to be highly accurate and to possess a strong independent prognostic value regardless of the field strength used.[54,55]

MYOCARDIAL MAPPING

In contrast to standard MRI approaches that are weighted toward specific relaxation parameters (T_1-weighted, T_2-weighted, etc),

parametric mapping techniques enable spatial visualization of tissue relaxation parameters such as T_1, T_2, and T_2* and respective possible quantitative changes thereof. Such strategies specifically help identification of diffuse processes where weighted imaging is unable to gather further insight. The benefits and potential challenges of such approaches have extensively been evaluated in recent years.

Although there is a variety of various technical approaches for myocardial T_1 mapping available, currently, modified Look-Locker inversion recovery (MOLLI) techniques are most commonly in use.[56,57] Although MOLLI offers excellent T_1 precision, it is sensitive to various influencing factors that include, among other, inversion pulse efficiency, magnetization transfer, and T_2 relaxation effects. This results in a reduced accuracy and underestimated T_1 times.[41,58,59] Furthermore, it is generally recommended to optimize the inversion grouping of MOLLI for specific ranges of T_1 values, for example, pre-GBCA and post-GBCA administration.[59] Alternative IR techniques that avoid the need for such "adjustments" include "shortened MOLLI" (ShMOLLI) and inversion group fitting MOLLI.[60,61] Saturation-prepared approaches, such as SASHA,[62] demonstrate increased popularity due to the much-improved accuracy and lack magnetization transfer and T_2 relaxation effects. Although initially demonstrating inferior precision, more recent developments and data have demonstrated further improved precision.[63]

Independent of the techniques in use, absolute results and reference ranges are generally only valid for a specific system as further influencing factors include the detailed pulse structures and gradient linearity. Thus, even when using MOLLI techniques on different manufacturers' scanners, results differ.

With the more common use of 3-T systems in cardiac MRI in recent years, there is also an increasing body of literature available in T_1 mapping at 3 T. As mentioned previously, the general increase in field strength from 1.5 T to 3 T results in a prolongation of T_1 relaxation times. Gottbrecht et al[64] had recently demonstrated this in a large meta-analysis including 120 studies using MOLLI, and a similar increase has been demonstrated for saturation-prepared methods (eg, SASHA).[63] The generally increased SNR at 3 T also may improve the precision of quantification of T_1 relaxation times and parametric map quality.[65,66] In particular, SASHA benefits of the increased SNR at 3 T with a drastically reduced loss in precision.[63] Further improvement of SASHA-based approaches results in precision similar to MOLLI and may also allow multiparametric single breath-hold approaches (mSASHA).

Despite the previously highlighted overall benefits of most T_1 mapping techniques at 3 T, some impacts of higher field strength have to be carefully considered. With the increased B_0 inhomogeneity at 3 T, off-resonance artifacts in SSFP-based readout techniques are of higher concern. As such, careful advanced shimming methods are essential not only to avoid visibly image artifacts but also to ensure appropriate and accurate fitting.[67]

In addition to quantification of the longitudinal relaxation time T_1, also quantification of the transverse relaxation time T_2 (eg, T_2 mapping) is increasingly performed to especially assess for inflammation and increased tissue water content (eg, edema). This is typically in addition to T_2-weighted imaging but also to complement T_1 mapping for combined interpretation of results. For T_2 mapping, typically a series of T_2-weighted images with different echo times or T_2 preparation times are acquired using a TSE sequence,[68] a T_2-prepared bSSFP[69] or spoiled GRE[70] sequence, or a gradient spin echo (GRASE) sequence combining spin echo excitation with GRE readout.[71]

Although T_2 mapping is also feasible at 3 T, in contrast to T_1 relaxation times, T_2 relaxation times decrease with increase in field strength. Compared with spin echo–based methods, the bSSFP readout is more sensitive to inhomogeneities in the main magnetic field and thus leading to slightly lower T_2 times. Particularly at 3 T, differences to up to 15% may be experienced when using T_2-prepared bSSFP sequences compared with reference standard multiecho TSE sequences.[72] In addition, it is important to keep in mind that for the application of T_2-prepared methods at 3 T, SAR constraints may limit the number of refocusing pulses. This also results in an increased susceptibility for T_2* effects and thus contributes to shorter T_2 times at 3 T for these methods. A change of readout techniques from SSFP to GRE may help obliviate this aspect. At 3 T, higher pixel-by-pixel homogeneity of T_2 values can be observed for GRASE and T_2-prepared methods, which may prove advantageous for threshold-based analysis of areas with pathological T_2 values.[72] Although it has generally been observed that T_2-prepared methods demonstrate the least artifacts at 1.5 T, GRASE-based methods showed the least artifacts among various techniques at 3 T. Nevertheless, it remains of high importance to appropriately assess for any artifact that may have appeared on either field strength to avoid misinterpretation.

As a third quantitative parameter of myocardial tissue characterization, T_2* assessment has long been established as a clinically important technique before the efforts in myocardial T_1 and T_2 quantification. The evaluation of myocardial T_2* relaxation times is considered the method of choice and standard of care for assessment of potential myocardial tissue iron overload.[73] This is specifically of high importance in patient populations with hemoglobinopathies such as thalassemia syndromes and structural hemoglobin variants. In recent years, applied techniques have also incorporated automated pixel-based analysis referred to as T_2* mapping. The acquisition is performed using a segmented GRE sequence generating a series of images (typically 8) with increasing echo times (~2–18 milliseconds). Although both bright-blood[74] and a black-blood[75] techniques have been validated and are widely used clinically, black-blood techniques demonstrate less prominent artifacts, less bias, and reduced interobserver variability.[76] If available, the black-blood technique with its double IR pulse is recommended.[77] Similar to T_2 relaxation, also T_2* relaxation times decrease with increasing field strength. Although at 1.5 T, T_2* values of >20 milliseconds are generally considered normal and indicating no clinically relevant iron; based on experiments, such cutoff is set to >12 milliseconds at 3 T.[78] As such, given the reduced range of possibly assessable T_2* values when considering the applied range of echo times, appropriate differentiation of mild, moderate, and severe iron overload might be hampered at 3 T. Given the intrinsically high sensitivity of T_2* techniques to susceptibility artifacts, which are specifically prominent along the lateral wall due to the proximity of the lung (eg, air) as well as in areas of larger cardiac vein structures along the anterior and posterior interventricular groove, the measurement of myocardial T_2* is generally restricted to the septum.[2,67]

Although myocardial T_2* quantification is generally feasible and reproducible at 3 T, the more prominent susceptibility artifacts that can generally be observed at 3 T lead to suboptimal accuracy and may also hamper segmental measurements of myocardial iron levels.[79] As such, myocardial T_2* assessment for the purpose of myocardial iron overload assessment does generally not benefit from higher field strength and should be performed at 1.5 T.[2] However, identification of subtle iron deposits, which may occur in hemorrhage of myocardial infarcts or even iron-based cell labeling in stem cell research may benefit of the generally higher sensitivity of 3 T to iron-induced susceptibility.

Independent of any of the above, it remains essential to obtain individual institutional reference values for T_1 and T_2 relaxation times at 1.5 T and 3 T using the identical sequence parameters as in the clinical population. Although benchmarking against published normal ranges may be beneficial, such approach is only appropriate in case the detailed acquisition parameters and used hardware are identical.[67] It is of crucial importance to understand that identical parameters used on different vendors' hardware will result in different quantitative T_1 and T_2 results. In addition, vendors operate at slightly different field strength, which is specifically obvious at high field strength (eg, 3 T) where the field strength may vary by up to 4% and as such directly affects longitudinal and transverse relaxation time constants.

Given the overall increased heterogeneity and more prominent artifacts at higher field strengths, quantitative image biomarker

assessment at 3 T requires more sophisticated and more careful shimming procedures aiming at both the main magnetic field and the RF field.

With respect to its clinical use, further studies are required to specifically investigate the prognostic and diagnostic values of T_1 and T_2 mapping at the single patient level in a broad range of pathologies. In patients with a specific disease such as Anderson-Fabry disease, especially T_1 mapping has already demonstrated its ability to improve the differential diagnosis of hypertrophic phenotypes and may also provide additional value in therapy monitoring of this disease.

PHASE-CONTRAST FLOW IMAGING

The ability of imaging moving spins, particularly vascular and also intracardiac blood flow, and to accurately quantify flow velocities and volumes is among the fairly unique abilities of phase contrast (PC) MRI. In PC techniques, protons accumulate an MR phase shift proportional to the speed at which they move along a magnetic gradient field. Subsequently, this information is used to generate an image contrast between these moving protons (eg, blood) and surrounding stationary protons (eg, soft tissues). Phase contrast techniques have long played a critical role not only in the assessment of valvular stenosis and shunt disease but also in the assessment of complex congenital heart disease. Based on spoiled GRE sequence techniques, PC MRI generally also benefits from the overall SNR boost at 3 T. Although the impact of higher field strength on general PC flow imaging is discussed in greater detail elsewhere,[80,81] we will specifically focus on a more recent iteration of these techniques, 4-dimensional (4D) PC flow imaging.

Four-dimensional PC flow imaging is a rapidly evolving technique that is gaining increased attention. In contrast to 2D techniques, it combines functional flow information over time with a 3D anatomical display. This is accomplished by time-resolved 3D 3-directionally encoded velocity data[82] offering a fourth dimension for visualization and quantification of (complex) flow patterns and flow-derived hemodynamics. Flow velocities, flow volumes, and wall shear stress could provide additional and potentially complementary information for clinical guidance and therapy. Four-dimensional PC flow offers a comprehensive overview and potentially new insights into the pathophysiology of different disease entities (eg, aortic aneurysms,[83] mitral and aortic valve pathology,[84,85] intracardiac pathology[86]) and might ultimately help to predict disease outcome and patient prognosis.[87,88] Detailed protocol recommendations for cardiac[89] and aortic[90] 4D flow can be found elsewhere.

For valvular heart disease, accurate and consistent quantification of valvular flow and regurgitation jets was shown across centers, scanners (1.5 T and 3 T), as well as MR protocols.[91] Strecker et al[92] demonstrated superior imaging quality for 3 T compared with 1.5 T in flow-sensitive 4D MRI in 10 healthy volunteers with no significant difference in quantitative values. The stability of measurements in 4D PC flow MRI across platforms and at different magnetic field strengths (1.5 T and 3 T) has recently been confirmed in another series.[93]

An intraindividual comparison of 4D PC flow at different field strengths at 1.5 T, 3 T, and 7 T in 10 healthy volunteers was published recently.[94] In this series, scan time was the longest at 7 T and varied substantially between approximately 8 and 15 minutes. The reason for such a large range is given by the navigator that failed in 5 of 10 subjects at 7 T due to insufficient B_1 magnitude to detect the position of the diaphragm. Nearly all aortic segments with nondiagnostic image quality were obtained at 7 T as well (9 of 10). In wall shear stress analysis, special attention has to be paid to changes in sequence or field strength during follow-up, as these varieties might lead to misinterpretation in patients with mild or moderate aortic stenosis. According to Wiesemann et al,[94] it is crucial to foster the clinical use of 4D PC MR, to establish if sequences/field strengths can be changed for a patient's follow-up investigation without affecting results, given the current lack of standardization.

DISCUSSION

Although 1.5 T magnetic field strength had been the predominant setting for cardiac MRI for over a decade, the ever-increasing drive toward high-field (eg, 3 T) scanner hardware has pushed the envelope for 3-T cardiac MRI. It has been well recognized that the general increase in SNR at 3 T, which has been the reason for other subspecialty MRI (eg, musculoskeletal, neuro, etc) moving toward 3 T, can also be used to an advantage for most cardiac MRI applications. This specifically holds true for first-pass perfusion and LGE imaging. The gain in SNR can be beneficial on its own or, alternatively, can also be (partly) traded for increased temporal or spatial resolution, or shorter scan times.

However, the increase in field strength comes along with new challenges that predominately relate to the increase in RF power deposition, as well as the increased B_0 and B_1 inhomogeneity. Particularly, imaging techniques that typically use high flip angles or techniques that are susceptible to inhomogeneities may pose challenges. In cardiac MRI, specifically bSSFP techniques are affected by these challenges. In

TABLE 1. Overview of the Preferred Field Strength for Various Cardiac MRI Applications

Application	Preference			Comments
	1.5 T	Either	3 T	
Functional imaging		X		• Increased image contrast can be appreciated at 3 T when imaging postcontrast administration • Banding artifacts may degrade overall image quality at 3 T
Edema imaging		X		
LGE		X	X	• Increased SNR at 3 T can be beneficial
Stress perfusion		X	X	• Increased SNR at 3 T can be beneficial
T_1 mapping		X		
T_2 mapping		X		
T_2* mapping	X			• Subdivision for iron overload severity more reliable at 1.5 T • 3 T may be used for higher sensitivity for any condition causing magnetic susceptibility
Flow imaging		X		• Increased SNR at 3 T beneficial for 4D flow
CIED, neurogenerators, other metal implants/devices	X			• Large portion of active/passive devices/implants only labeled MR conditional at 1.5 T

CIED, cardiac implantable electronic device.

cine imaging, this may result in slightly reduced contrast between blood-pool and myocardium (due to the need of reduced flip angles) as well as more common and/or more prominent off-resonance artifacts. Advanced high-order B_0 and B_1 shimming methods help to overcome the latter. Furthermore, MRI systems with multiple RF transmitters (multitransmit systems) can further improve RF homogeneity.

Most importantly, the transition to 3-T cardiac MRI requires optimization of imaging methods with adaptation to accompanying changes in relaxation and other high-field effects. Simple transfer of 1.5 T protocols for use at 3 T will not suffice. This is specifically of importance in all quantitative imaging techniques to optimize accuracy and precision, keeping in mind the variation in exact field strength that different manufacturers are operating in the 3-T bracket.

Another important consideration is the interaction and safety of active and passive implants. This does not only include cardiac implantable electronic devices (CIEDs; eg, pacemakers, automated implantable cardioverter defibrillators) and stents but also implanted neurogenerators (eg, deep brain stimulator, etc) and all metal containing implants that cannot be removed before MRI. Although devices/implants may primarily cause disturbances in the magnetic field and thereby create imaging artifacts possibly rendering images nondiagnostic, interactions with the various MR components may also affect electronics of such devices or induce currents in the device/implant, potentially leading to heat-related tissue damage. Although many devices have been tested and are considered safe under specific conditions (MR conditional) at 1.5 T, testing for 3 T conditional status is less common, although the list is slowly expanding.[95] Individual factors, including the configuration, orientation and position of leads, the length and extension of the lead relative to the transmitter coil, and the anatomic region imaged, will influence the potential heating as well. Field strength, therefore, is relevant, but not a sole determining factor. Appropriate MR safety screening by appropriately educated and trained personnel, and detailed planning and preparation with appropriate scan conditions are key in this respect. In any case, patient and referring physician should be informed and instructed before the examination. With respect to metal implant-induced artifacts, the use of wideband sequences may help minimize those and improve diagnostic image quality at both 1.5 T[96] and 3 T.[97]

More recently, other field strengths have undergone exploration for potential use in cardiac MRI. The quest for spatial resolution at high SNR has pushed the use of ultra-high field strengths (eg, 7 T) in particular for neuroimaging but has also expanded into the exploration of cardiac applications.[94] At the opposite end of the spectrum, most recently, new low field strength (<1 T) systems have been explored recently.[98] In general, such low field systems, fitted with modern gradient systems and receiver array coils, use artificial intelligence architectures and algorithms in order to overcome field-related limited SNR. If successful in the overall field of cardiac MRI applications, such systems would be highly attractive due to their significant lower costs, excellent field homogeneity, and the fact that energy deposition no longer poses issues.

With an increasing number of clinical cardiac applications,[99] with each having their own advantages at both field strengths, no "holy grail" field strength exists for cardiac MRI (Table 1). Ideally, having both field strengths available enables referring patients to the most "ideal" field strength based on the requested cardiac applications. However, in case only a single MR system can be used for cardiac MRI, 1.5 T would still be our preferred field strength regarding the compatibility with all major clinical cardiac applications, ease of use, and accessibility for an increasing number of patients with cardiac devices/implants.

REFERENCES

1. Singerman RW, Denison TJ, Wen H, et al. Simulation of B1 field distribution and intrinsic signal-to-noise in cardiac MRI as a function of static magnetic field. *J Magn Reson*. 1997;125:72–83.
2. Kramer CM, Barkhausen J, Bucciarelli-Ducci C, et al. Standardized cardiovascular magnetic resonance imaging (CMR) protocols: 2020 update. *J Cardiovasc Magn Reson*. 2020;22:17.
3. Bieri O, Scheffler K. Fundamentals of balanced steady state free precession MRI. *J Magn Reson Imaging*. 2013;38:2–11.
4. Hudsmith LE, Cheng AS, Tyler DJ, et al. Assessment of left atrial volumes at 1.5 Tesla and 3 Tesla using FLASH and SSFP cine imaging. *J Cardiovasc Magn Reson*. 2007;9:673–679.
5. Maroules CD, McColl R, Khera A, et al. Interstudy reproducibility of SSFP cine magnetic resonance: impact of magnetic field strength and parallel imaging. *J Magn Reson Imaging*. 2008;27:1139–1145.
6. Wieben O, Francois C, Reeder SB. Cardiac MRI of ischemic heart disease at 3 T: potential and challenges. *Eur J Radiol*. 2008;65:15–28.
7. Soher BJ, Dale BM, Merkle EM. A review of MR physics: 3T versus 1.5T. *Magn Reson Imaging Clin N Am*. 2007;15:277–290, v.
8. Oshinski JN, Delfino JG, Sharma P, et al. Cardiovascular magnetic resonance at 3.0 T: current state of the art. *J Cardiovasc Magn Reson*. 2010;12:55.
9. Childs AS, Malik SJ, O'Regan DP, et al. Impact of number of channels on RF shimming at 3T. *MAGMA*. 2013;26:401–410.
10. Deshpande VS, Shea SM, Li D. Artifact reduction in true-FISP imaging of the coronary arteries by adjusting imaging frequency. *Magn Reson Med*. 2003;49:803–809.
11. Malayeri AA, Johnson WC, Macedo R, et al. Cardiac cine MRI: quantification of the relationship between fast gradient echo and steady-state free precession for determination of myocardial mass and volumes. *J Magn Reson Imaging*. 2008;28:60–66.
12. Stillman AE, Wilke N, Jerosch-Herold M. Use of an intravascular T1 contrast agent to improve MR cine myocardial-blood pool definition in man. *J Magn Reson Imaging*. 1997;7:765–767.
13. Celutkiene J, Plymen CM, Flachskampf FA, et al. Innovative imaging methods in heart failure: a shifting paradigm in cardiac assessment. Position statement on behalf of the Heart Failure Association of the European Society of Cardiology. *Eur J Heart Fail*. 2018;20:1615–1633.
14. Zerhouni EA, Parish DM, Rogers WJ, et al. Human heart: tagging with MR imaging—a method for noninvasive assessment of myocardial motion. *Radiology*. 1988;169:59–63.
15. Osman NF, Sampath S, Atalar E, et al. Imaging longitudinal cardiac strain on short-axis images using strain-encoded MRI. *Magn Reson Med*. 2001;46:324–334.
16. Aletras AH, Ding S, Balaban RS, et al. DENSE: displacement encoding with stimulated echoes in cardiac functional MRI. *J Magn Reson*. 1999;137:247–252.
17. Lim C, Blaszczyk E, Riazy L, et al. Quantification of myocardial strain assessed by cardiovascular magnetic resonance feature tracking in healthy subjects—influence of segmentation and analysis software. *Eur Radiol*. 2021;31:3962–3972.
18. Schuster A, Morton G, Hussain ST, et al. The intra-observer reproducibility of cardiovascular magnetic resonance myocardial feature tracking strain assessment is independent of field strength. *Eur J Radiol*. 2013;82:296–301.
19. Barreiro-Perez M, Curione D, Symons R, et al. Left ventricular global myocardial strain assessment comparing the reproducibility of four commercially available CMR-feature tracking algorithms. *Eur Radiol*. 2018;28:5137–5147.
20. Backhaus SJ, Metschies G, Billing M, et al. Cardiovascular magnetic resonance imaging feature tracking: impact of training on observer performance and reproducibility. *PLoS One*. 2019;14:e0210127.
21. Kloner RA, Rude RE, Carlson N, et al. Ultrastructural evidence of microvascular damage and myocardial cell injury after coronary artery occlusion: which comes first? *Circulation*. 1980;62:945–952.
22. Dall'Armellina E, Karia N, Lindsay AC, et al. Dynamic changes of edema and late gadolinium enhancement after acute myocardial infarction and their relationship to functional recovery and salvage index. *Circ Cardiovasc Imaging*. 2011;4:228–236.
23. Simonetti OP, Finn JP, White RD, et al. "Black blood" T2-weighted inversion-recovery MR imaging of the heart. *Radiology*. 1996;199:49–57.
24. Kellman P, Aletras AH, Mancini C, et al. T2-prepared SSFP improves diagnostic confidence in edema imaging in acute myocardial infarction compared to turbo spin echo. *Magn Reson Med*. 2007;57:891–987.
25. Aletras AH, Kellman P, Derbyshire JA, et al. ACUT2E TSE-SSFP: a hybrid method for T2-weighted imaging of edema in the heart. *Magn Reson Med*. 2008;59:229–235.
26. Zhu Y, Yang D, Zou L, et al. T2STIR preparation for single-shot cardiovascular magnetic resonance myocardial edema imaging. *J Cardiovasc Magn Reson*. 2019;21:72.
27. Simonetti OP, Kim RJ, Fieno DS, et al. An improved MR imaging technique for the visualization of myocardial infarction. *Radiology*. 2001;218:215–223.

28. Li W, Li BS, Polzin JA, et al. Myocardial delayed enhancement imaging using inversion recovery single-shot steady-state free precession: initial experience. *J Magn Reson Imaging*. 2004;20:327–330.
29. Huber A, Bauner K, Wintersperger BJ, et al. Phase-sensitive inversion recovery (PSIR) single-shot TrueFISP for assessment of myocardial infarction at 3 tesla. *Invest Radiol*. 2006;41:148–153.
30. Kellman P, Dyke CK, Aletras AH, et al. Artifact suppression in imaging of myocardial infarction using B1-weighted phased-array combined phase-sensitive inversion recovery. *Magn Reson Med*. 2004;51:408–412.
31. Captur G, Lobascio I, Ye Y, et al. Motion-corrected free-breathing LGE delivers high quality imaging and reduces scan time by half: an independent validation study. *Int J Cardiovasc Imaging*. 2019;35:1893–1901.
32. Holtackers RJ, Gommers S, Van De Heyning CM, et al. Steadily increasing inversion time improves blood suppression for free-breathing 3D late gadolinium enhancement MRI with optimized dark-blood contrast. *Invest Radiol*. 2021; 56:335–340.
33. Pennig L, Lennartz S, Wagner A, et al. Clinical application of free-breathing 3D whole heart late gadolinium enhancement cardiovascular magnetic resonance with high isotropic spatial resolution using compressed SENSE. *J Cardiovasc Magn Reson*. 2020;22:89.
34. Munoz C, Bustin A, Neji R, et al. Motion-corrected 3D whole-heart water-fat high-resolution late gadolinium enhancement cardiovascular magnetic resonance imaging. *J Cardiovasc Magn Reson*. 2020;22:53.
35. Klumpp B, Fenchel M, Hoevelborn T, et al. Assessment of myocardial viability using delayed enhancement magnetic resonance imaging at 3.0 Tesla. *Invest Radiol*. 2006;41:661–667.
36. Bauner KU, Muehling O, Wintersperger BJ, et al. Inversion recovery single-shot TurboFLASH for assessment of myocardial infarction at 3 Tesla. *Invest Radiol*. 2007;42:361–371.
37. Ligabue G, Fiocchi F, Ferraresi S, et al. 3-Tesla MRI for the evaluation of myocardial viability: a comparative study with 1.5-Tesla MRI. *Radiol Med*. 2008;113: 347–362.
38. Rohrer M, Bauer H, Mintorovitch J, et al. Comparison of magnetic properties of MRI contrast media solutions at different magnetic field strengths. *Invest Radiol*. 2005;40:715–724.
39. Sharma P, Socolow J, Patel S, et al. Effect of Gd-DTPA-BMA on blood and myocardial T1 at 1.5T and 3T in humans. *J Magn Reson Imaging*. 2006;23:323–330.
40. Gutberlet M, Noeske R, Schwinge K, et al. Comprehensive cardiac magnetic resonance imaging at 3.0 Tesla: feasibility and implications for clinical applications. *Invest Radiol*. 2006;41:154–167.
41. Kellman P, Herzka DA, Hansen MS. Adiabatic inversion pulses for myocardial T1 mapping. *Magn Reson Med*. 2014;71:1428–1434.
42. Fahmy AS, Neisius U, Tsao CW, et al. Gray blood late gadolinium enhancement cardiovascular magnetic resonance for improved detection of myocardial scar. *J Cardiovasc Magn Reson*. 2018;20:22.
43. Holtackers RJ, Van De Heyning CM, Nazir MS, et al. Clinical value of dark-blood late gadolinium enhancement cardiovascular magnetic resonance without additional magnetization preparation. *J Cardiovasc Magn Reson*. 2019;21:44.
44. Kim HW, Rehwald WG, Jenista ER, et al. Dark-blood delayed enhancement cardiac magnetic resonance of myocardial infarction. *JACC Cardiovasc Imaging*. 2018;11:1758–1769.
45. Polacin M, Gastl M, Kapos I, et al. Novel magnetic resonance late gadolinium enhancement with fixed short inversion time in ischemic myocardial scars. *Invest Radiol*. 2020;55:445–450.
46. Holtackers RJ, Van De Heyning CM, Chiribiri A, et al. Dark-blood late gadolinium enhancement CMR for improved detection of subendocardial scar: a review of current techniques. *J Cardiovasc Magn Reson*. 2021. In press.
47. Plein S, Greenwood JP, Ridgway JP. *Cardiovascular MR Manual*. London, United Kingdom/New York, NY: Springer; 2011:487.
48. Theisen D, Wintersperger BJ, Huber A, et al. Myocardial perfusion imaging with gadobutrol: a comparison between 3 and 1.5 Tesla with an identical sequence design. *Invest Radiol*. 2007;42:499–506.
49. Lockie T, Ishida M, Perera D, et al. High-resolution magnetic resonance myocardial perfusion imaging at 3.0-Tesla to detect hemodynamically significant coronary stenoses as determined by fractional flow reserve. *J Am Coll Cardiol*. 2011;57:70–75.
50. Cheng AS, Pegg TJ, Karamitsos TD, et al. Cardiovascular magnetic resonance perfusion imaging at 3-Tesla for the detection of coronary artery disease: a comparison with 1.5-Tesla. *J Am Coll Cardiol*. 2007;49:2440–2449.
51. Min JY, Ko SM, Song IY, et al. Comparison of the diagnostic accuracies of 1.5T and 3T stress myocardial perfusion cardiovascular magnetic resonance for detecting significant coronary artery disease. *Korean J Radiol*. 2018;19: 1007–1020.
52. Hsu LY, Jacobs M, Benovoy M, et al. Diagnostic performance of fully automated pixel-wise quantitative myocardial perfusion imaging by cardiovascular magnetic resonance. *JACC Cardiovasc Imaging*. 2018;11:697–707.
53. Scannell CM, Veta M, Villa ADM, et al. Deep-learning-based preprocessing for quantitative myocardial perfusion MRI. *J Magn Reson Imaging*. 2020;51: 1689–1696.
54. Sammut EC, Villa ADM, Di Giovine G, et al. Prognostic value of quantitative stress perfusion cardiac magnetic resonance. *JACC Cardiovasc Imaging*. 2018; 11:686–694.
55. Knott KD, Seraphim A, Augusto JB, et al. The prognostic significance of quantitative myocardial perfusion: an artificial intelligence-based approach using perfusion mapping. *Circulation*. 2020;141:1282–1291.
56. Messroghli DR, Greiser A, Frohlich M, et al. Optimization and validation of a fully-integrated pulse sequence for modified look-locker inversion-recovery (MOLLI) T1 mapping of the heart. *J Magn Reson Imaging*. 2007;26:1081–1086.
57. Messroghli DR, Radjenovic A, Kozerke S, et al. Modified Look-Locker inversion recovery (MOLLI) for high-resolution T1 mapping of the heart. *Magn Reson Med*. 2004;52:141–146.
58. Robson MD, Piechnik SK, Tunnicliffe EM, et al. T1 measurements in the human myocardium: the effects of magnetization transfer on the SASHA and MOLLI sequences. *Magn Reson Med*. 2013;70:664–770.
59. Kellman P, Hansen MS. T1-mapping in the heart: accuracy and precision. *J Cardiovasc Magn Reson*. 2014;16:2.
60. Piechnik SK, Ferreira VM, Dall'Armellina E, et al. Shortened Modified Look-Locker Inversion recovery (ShMOLLI) for clinical myocardial T1-mapping at 1.5 and 3 T within a 9 heartbeat breathhold. *J Cardiovasc Magn Reson*. 2010;12:69.
61. Sussman MS, Wintersperger BJ. Modified look-locker inversion recovery (MOLLI) T_1 mapping with inversion group (IG) fitting—a method for improved precision. *Magn Reson Imaging*. 2019;62:38–45.
62. Chow K, Flewitt JA, Green JD, et al. Saturation recovery single-shot acquisition (SASHA) for myocardial T(1) mapping. *Magn Reson Med*. 2014;71:2082–2095.
63. Weingärtner S, Meßner NM, Budjan J, et al. Myocardial T1-mapping at 3T using saturation-recovery: reference values, precision and comparison with MOLLI. *J Cardiovasc Magn Reson*. 2016;18:84.
64. Gottbrecht M, Kramer CM, Salerno M. Native T1 and extracellular volume measurements by cardiac MRI in healthy adults: a meta-analysis. *Radiology*. 2019; 290:317–326.
65. Dabir D, Child N, Kalra A, et al. Reference values for healthy human myocardium using a T1 mapping methodology: results from the international T1 multicenter cardiovascular magnetic resonance study. *J Cardiovasc Magn Reson*. 2014;16:69.
66. von Knobelsdorff-Brenkenhoff F, Prothmann M, Dieringer MA, et al. Myocardial T1 and T2 mapping at 3 T: reference values, influencing factors and implications. *J Cardiovasc Magn Reson*. 2013;15:53.
67. Messroghli DR, Moon JC, Ferreira VM, et al. Clinical recommendations for cardiovascular magnetic resonance mapping of T1, T2, T2* and extracellular volume: a consensus statement by the Society for Cardiovascular Magnetic Resonance (SCMR) endorsed by the European Association for Cardiovascular Imaging (EACVI). *J Cardiovasc Magn Reson*. 2017;19:75.
68. McNamara MT, Higgins CB, Schechtmann N, et al. Detection and characterization of acute myocardial infarction in man with use of gated magnetic resonance. *Circulation*. 1985;71:717–724.
69. Huang TY, Liu YJ, Stemmer A, et al. T2 measurement of the human myocardium using a T2-prepared transient-state TrueFISP sequence. *Magn Reson Med*. 2007; 57:960–966.
70. Foltz WD, Al-Kwifi O, Sussman MS, et al. Optimized spiral imaging for measurement of myocardial T2 relaxation. *Magn Reson Med*. 2003;49:1089–1097.
71. Sprinkart AM, Luetkens JA, Traber F, et al. Gradient spin echo (GraSE) imaging for fast myocardial T2 mapping. *J Cardiovasc Magn Reson*. 2015;17:12.
72. Baeßler B, Schaarschmidt F, Stehning C, et al. A systematic evaluation of three different cardiac T2-mapping sequences at 1.5 and 3T in healthy volunteers. *Eur J Radiol*. 2015;84:2161–2170.
73. Brittenham GM. Iron-chelating therapy for transfusional iron overload. *N Engl J Med*. 2011;364:146–156.
74. Westwood M, Anderson LJ, Firmin DN, et al. A single breath-hold multiecho T2* cardiovascular magnetic resonance technique for diagnosis of myocardial iron overload. *J Magn Reson Imaging*. 2003;18:33–39.
75. He T, Gatehouse PD, Kirk P, et al. Black-blood T2* technique for myocardial iron measurement in thalassemia. *J Magn Reson Imaging*. 2007;25: 1205–1209.
76. Smith GC, Carpenter JP, He T, et al. Value of black blood T2* cardiovascular magnetic resonance. *J Cardiovasc Magn Reson*. 2011;13:21.

77. Pennell DJ, Udelson JE, Arai AE, et al. Cardiovascular function and treatment in β-thalassemia major: a consensus statement from the American Heart Association. *Circulation*. 2013;128:281–308.
78. Triadyaksa P, Oudkerk M, Sijens PE. Cardiac T2 * mapping: Techniques and clinical applications. *J Magn Reson Imaging*. 2020;52:1340–1351.
79. Meloni A, Positano V, Keilberg P, et al. Feasibility, reproducibility, and reliability for the T*2 iron evaluation at 3 T in comparison with 1.5 T. *Magn Reson Med*. 2012;68:543–551.
80. Lotz J, Doker R, Noeske R, et al. In vitro validation of phase-contrast flow measurements at 3 T in comparison to 1.5 T: precision, accuracy, and signal-to-noise ratios. *J Magn Reson Imaging*. 2005;21:604–610.
81. Nayak KS, Nielsen JF, Bernstein MA, et al. Cardiovascular magnetic resonance phase contrast imaging. *J Cardiovasc Magn Reson*. 2015;17:71.
82. Markl M, Frydrychowicz A, Kozerke S, et al. 4D flow MRI. *J Magn Reson Imaging*. 2012;36:1015–1036.
83. Ramaekers MJFG, Adriaans BP, Juffermans JF, et al. Characterization of ascending aortic flow in patients with degenerative aneurysms: a 4D flow magnetic resonance study. *Invest Radiol*. 2021.
84. Fidock B, Archer G, Barker N, et al. Standard and emerging CMR methods for mitral regurgitation quantification. *Int J Cardiol*. 2021;331:316–321.
85. Adriaans BP, Westenberg JJM, van Cauteren YJM, et al. Clinical assessment of aortic valve stenosis: comparison between 4D flow MRI and transthoracic echocardiography. *J Magn Reson Imaging*. 2020;51:472–480.
86. Rizk J. 4D flow MRI applications in congenital heart disease. *Eur Radiol*. 2021; 31:1160–1174.
87. Calkoen EE, de Koning PJ, Blom NA, et al. Disturbed intracardiac flow organization after atrioventricular septal defect correction as assessed with 4D flow magnetic resonance imaging and quantitative particle tracing. *Invest Radiol*. 2015;50:850–857.
88. Adriaans BP, Wildberger JE, Westenberg JJM, et al. Predictive imaging for thoracic aortic dissection and rupture: moving beyond diameters. *Eur Radiol*. 2019; 29:6396–6404.
89. Zhong L, Schrauben EM, Garcia J, et al. Intracardiac 4D flow MRI in congenital heart disease: recommendations on behalf of the ISMRM Flow & Motion Study Group. *J Magn Reson Imaging*. 2019;50:677–681.
90. Dyverfeldt P, Bissell M, Barker AJ, et al. 4D flow cardiovascular magnetic resonance consensus statement. *J Cardiovasc Magn Reson*. 2015;17:72.
91. Juffermans JF, Minderhoud SCS, Wittgren J, et al. Multicenter consistency assessment of valvular flow quantification with automated valve tracking in 4D flow CMR. *JACC Cardiovasc Imaging*. 2021.
92. Strecker C, Harloff A, Wallis W, et al. Flow-sensitive 4D MRI of the thoracic aorta: comparison of image quality, quantitative flow, and wall parameters at 1.5 T and 3 T. *J Magn Reson Imaging*. 2012;36:1097–1103.
93. Ebel S, Dufke J, Köhler B, et al. Automated quantitative extraction and analysis of 4D flow patterns in the ascending aorta: an intraindividual comparison at 1.5 T and 3 T. *Sci Rep*. 2020;10:2949.
94. Wiesemann S, Schmitter S, Demir A, et al. Impact of sequence type and field strength (1.5, 3, and 7T) on 4D flow MRI hemodynamic aortic parameters in healthy volunteers. *Magn Reson Med*. 2021;85:721–733.
95. http://www.mrisafety.com/index.html. Accessed March 30, 2021.
96. Do DH, Eyvazian V, Bayoneta AJ, et al. Cardiac magnetic resonance imaging using wideband sequences in patients with nonconditional cardiac implanted electronic devices. *Heart Rhythm*. 2018;15:218–225.
97. Ranjan R, McGann CJ, Jeong EK, et al. Wideband late gadolinium enhanced magnetic resonance imaging for imaging myocardial scar without image artefacts induced by implantable cardioverter-defibrillator: a feasibility study at 3 T. *Europace*. 2015;17:483–488.
98. Bandettini WP, Shanbhag SM, Mancini C, et al. A comparison of cine CMR imaging at 0.55 T and 1.5 T. *J Cardiovasc Magn Reson*. 2020;22:37.
99. Emrich T, Halfmann M, Schoepf UJ, et al. CMR for myocardial characterization in ischemic heart disease: state-of-the-art and future developments. *Eur Radiol Exp*. 2021;5:14.